Eur. J. Mineral., 37, 699–708, 2025
https://doi.org/10.5194/ejm-37-699-2025

European Journal of Mineralogy
Open Access

High-pressure behaviour of a $CaIrO_3$ perovskite-type structure

Tiziana Boffa Ballaran[1], Kanchana Kularatne[1,2], and Reidar G. Trønnes[3]

[1]Bayerisches Geoinstitut, Universität Bayreuth, 95440 Bayreuth, Germany
[2]Laboratoire des Fluides Complexes et leurs Réservoirs, Université de Pau et des Pays de l'Adour, E2S UPPA, CNRS, LFCR, Pau, France
[3]Natural History Museum and Centre for Planetary Habitability, University of Oslo, 0316 Oslo, Norway

Correspondence: Tiziana Boffa Ballaran (tiziana.boffa-ballaran@uni-bayreuth.de)

Received: 27 February 2025 – Revised: 9 July 2025 – Accepted: 13 July 2025 – Published: 10 October 2025

Abstract. Structural refinements of single-crystal X-ray diffraction data collected at room temperature both under ambient and under high pressures up to 10 GPa have been used to characterise the octahedral tilting and site distortions of the orthorhombic *Pbnm* $CaIrO_3$ perovskite-type phase. The octahedral tilting has been evaluated using both the unit-cell lattice parameters and the displacements of the oxygen and A site from their hypothetical positions in an ideal cubic perovskite structure. The difference between the two types of calculations shows that the assumption of rigid and undistorted octahedra made for determining the tilt angles from the unit-cell parameters is valid only as a first approximation, especially in the case of $CaRuO_3$, $CaRhO_3$ and $CaIrO_3$ perovskites, for which polyhedral distortions are significant. $CaIrO_3$ perovskite appears to have much larger tilting and distortion than other CaO perovskites, likely causing the structure to be stiffer than expected from the general trend of the bulk moduli defined by other CaO perovskites. Moreover, in contrast to other CaO perovskites for which the Ca polyhedron is more compressible than the octahedral site, the compressibility of the IrO_6 octahedra is very similar to that of the CaO_{12} polyhedra, giving rise to an octahedral tilting that is independent of pressure at least up to 10 GPa. This behaviour may help reduce the electronic interactions among oxygens of neighbouring octahedra during compression, given the already large tilts present in the $CaIrO_3$ perovskite structure, and it is likely responsible for the bulk modulus's first pressure derivative being smaller than 4. Larger tilting and distortions are also observed for CaO perovskites that have a Pt-group element occupying the octahedral site. Such perovskites have been found to undergo a phase transformation to an orthorhombic *Cmcm* post-perovskite phase ($CaIrO_3$-type structure) at pressures below 25 GPa, suggesting that a large octahedral tilting and polyhedral distortion may be a requisite for stabilising the orthorhombic post-perovskite phase of CaO perovskite-type materials.

1 Introduction

The discovery of a phase transition from orthorhombic *Pbnm* $MgSiO_3$ bridgmanite to an orthorhombic post-perovskite *Cmcm* phase (Murakami et al., 2004; Oganov and Ono, 2004) sparked major interest in the behaviour of $CaIrO_3$, which is isostructural with post-perovskite under ambient conditions and transforms to a perovskite-type structure at 1–3 GPa and temperatures > 1350 °C (McDaniel and Schneidler, 1972; Hirose and Fujita, 2005; Kojitani et al., 2007a; Stølen and Trønnes, 2007; Trønnes et al., 2006) and therefore can be used as an analogue of the high-pressure $MgSiO_3$ phases. However, the majority of studies have focused their attention on the behaviour of the *Cmcm* $CaIrO_3$ phase, whereas only one study (Cheng et al., 2011) has reported the structural data of the $CaIrO_3$ perovskite-type phase ($CaIrO_3$ pv) obtained from synchrotron X-ray powder diffraction. $CaIrO_3$ pv exhibits an orthorhombic *Pbnm* symmetry like many other CaO perovskites, which displays different degrees of distortion from the cubic aristotype perovskite structure $Pm\bar{3}m$. This distortion is described in terms of octahedral tilting

about the pseudo-cubic axes (Glazer, 1972). Several methods have been used in the literature to calculate the tilt angles of the orthorhombic perovskite structure. The simplest way is to make use of unit-cell lattice parameters (i.e. Mitchell, 2002; O'Keeffe et al., 1979; Zhao et al., 1993) under the assumption that the octahedra are rigid and undistorted and that the orthorhombic distortion is therefore due to only octahedral tilting. However, since the octahedral framework in orthorhombic perovskite is neither rigid nor regular, a more accurate description of the octahedral tilting and polyhedral distortion of the orthorhombic perovskite structure is obtained from symmetry-mode analysis with respect to the ideal cubic perovskite structure. Symmetry modes are collective correlated atomic displacements that follow specific symmetry properties (Perez-Mato et al., 2010). The structural distortion in orthorhombic perovskites can be decomposed into contributions from different modes with symmetries given by the irreducible representations (Irreps) of the cubic $Pm\bar{3}m$ aristotype structure (Howard and Stokes, 2002, 1998; Perez-Mato et al., 2010). Such decomposition allows the octahedral tilting to be separated from the B- and A-site distortions. Only Irreps at the following k points of the reciprocal space of the cubic perovskite needs to be considered: Γ (0, 0, 0), X (0, 0, $\frac{1}{2}$), M ($\frac{1}{2}$, $\frac{1}{2}$, 0) and R ($\frac{1}{2}$, $\frac{1}{2}$, $\frac{1}{2}$). Using the notation of Miller and Love (1967), Howard and Stokes (1998, 2002) have shown that the two Irreps R_4^+ and M_3^+ induce the out-of-phase and in-phase tilt patterns of the perovskite octahedral framework and that they are truly independent of the polyhedral distortion. For *Pbnm* perovskites, three more Irreps are indicated as secondary symmetry modes, since they do not drive the displacive phase transformation from the cubic to the orthorhombic structure. These modes (R_5^+, X_5^+ and M_2^+) usually have much smaller amplitudes with respect to the R_4^+ and M_3^+ primary modes and are responsible for the polyhedral distortion in orthorhombic perovskite. Moreover, whilst the R_4^+, M_3^+ and M_2^+ modes are related only to displacements of the oxygen atoms, the R_5^+ and X_5^+ modes are due to displacements of both the oxygen atoms and the Ca atoms occupying the A site. A sketch visualisation of the displacements of the oxygens and A-site cations from their ideal position in the cubic aristotype structure associated with the five symmetry-adapted modes is given in Huang et al. (2021).

For $CaB^{4+}O_3$ perovskites, with B representing the cation occupying the octahedral B site, we can expect that octahedral tilting and distortion vary systematically with the size of the B-site cations, since Ca always occupy the cavity (A site) of the three-dimensional octahedral framework. This hypothesis is supported by the fact that the variation in the isothermal bulk modulus (K_{T0}) of $CaB^{4+}O_3$ perovskites with the B cation being Zr, Sn, Ti and Ge falls on a single smooth trend versus the inverse of the molar volume (Ross and Chaplin, 2003), implying that for larger unit-cell volumes (i.e. at lower atom packing densities), the bulk modulus is lower and the perovskites are softer. However, the bulk modulus of $CaIrO_3$ pv determined both from compression experiments (Boffa Ballaran et al., 2007) and from ab initio calculations (Marbouh et al., 2021) is much higher than that of other CaO perovskites and plots above the trend reported by Ross and Chaplin (2003). Moreover, the first pressure derivative of the bulk modulus, K', is smaller than 4, whereas the other CaO perovskites have K' values close to 6. In order to shed light on the structural reasons for the anomalous stiffening of $CaIrO_3$ perovskite with respect to the other $CaB^{4+}O_3$ perovskite, we performed a high-pressure diffraction study on a single crystal of $CaIrO_3$ pv and obtained the variation in the crystal structure of this perovskite up to 10 GPa.

2 Experimental method

2.1 Single-crystal X-ray diffraction under ambient conditions and structural refinements

A single crystal of $CaIrO_3$ pv with dimensions $69 \times 86 \times 148\,\mu m^3$ (Ba8x2) was selected from the run product synthesised in a previous study (Trønnes et al., 2006) at 1525 °C and 2.5 GPa in a piston-cylinder apparatus from a starting mixture of high-purity $CaCO_3$ and IrO_2 decarbonated and sintered at 900–950 °C. A crystal from the same run product was used in the compressibility study performed by Boffa Ballaran et al. (2007). Full-intensity data collection for structural refinements under ambient conditions was performed using the Oxford Diffraction Xcalibur diffractometer equipped with a graphite monochromator; a ceramic X-ray tube with Mo radiation, operated at 50 kV and 40 mA; and a Sapphire 2 CCD detector. Complete and redundant intensity data were collected using ω scans with a width of 0.5° and a default time of 15 s up to $2\theta = 72.5°$. The intensity data were integrated using CrysAlisPro software (Oxford Diffraction, Rigaku), applying Lorentz and polarisation corrections. Given the large linear absorption coefficient of $CaIrO_3$ pv ($\mu = 60.05\,mm^{-1}$ for Mo radiation), an analytical absorption correction based on the crystal shape (Clark and Reid, 1995) was also performed together with an empirical correction, taking into account frame and detector area scaling. A total of 568 unique reflections were obtained, of which 526 have $I > 2\sigma(I)$, with a final discrepancy factor $R_{int} = 0.0557$. Systematic absences are consistent with the *Pbnm* space group, which has therefore been used to solve the $CaIrO_3$ pv structure using the SHELXS programme (Sheldrick, 2015). The Ir and Ca atomic positions were identified using the Patterson algorithm, whereas the oxygen positions in the asymmetric unit were found by analysing the difference electron density map. Structural refinements were performed using the SHELXL programme (Sheldrick, 2015) built in the ShelXle (Hübschle et al., 2011) graphical user interfaces. Neutral scattering factors for Ca, Ir and O were used, and all atoms were refined anisotropically. The crystallographic information file (CIF) is available in the Supplement.

2.2 High-pressure single-crystal X-ray diffraction and structural refinements

Unfortunately, the Ba8x2 crystal was lost while trying to cut it to produce a smaller crystal suited for the high-pressure experiment. Therefore, another crystal (Ba8x4) with dimensions $61 \times 34 \times 20\,\mu m^3$ was selected. A BX90-type diamond anvil cell (DAC) (Kantor et al., 2012), with diamond culets of 400 µm diameter glued into Boehler–Almax seats with an opening angle of 90°, was prepared with a Re gasket preindented to a thickness of ∼ 60 µm from its original thickness of 200 µm. A hole with a diameter of 200 µm was laser-cut into the centre of this indentation to produce the sample chamber. The $CaIrO_3$ crystal was loaded inside the DAC together with a small ruby sphere as a pressure calibrant (Shen et al., 2020). Neon gas was loaded into the DAC to act as a pressure-transmitting medium, using the gas-loading system installed at the BGI (Kurnosov et al., 2008). The DAC was left to stabilise after each pressure increase for at least 1 d before performing the XRD measurements. The ruby luminescence was measured before and after each XRD measurement by means of a Horiba LABRAM HR Raman microspectrometer equipped with an $1800\,gr\,mm^{-1}$ grating and a He–Ne laser ($\lambda = 632.8$ nm) with 20 mW laser power.

Intensity data for all accessible reflections were collected at room temperature and at six different pressure points, including ambient pressure in the DAC without a pressure medium up to 9.7 (1) GPa. Above this pressure, significant broadening of the reflections was observed, and therefore the experiment was interrupted. Data collection at different pressures was performed using ω scans with a step size of 1° in a fixed-φ mode (Finger and King, 1978) up to 63° in 2θ. Every frame was measured for 120 s. The intensity integration was performed using CrysAlisPro software (Oxford Diffraction, Rigaku), applying Lorentz and polarisation corrections. Absorption effects due to the sample and diamonds, as well as shadowing effects due to the gasket, have been taken into account using the Absorb programme (Angel, 2004) implemented in the CrysAlisPro software. Due to the DAC spatial limitation, the resulting number of unique reflections was 241 for the crystal in the DAC under ambient pressure and between 210 and 230 for the collections performed under high pressures. Structural refinements were performed using the SHELX programmes (Sheldrick, 2015) built in the ShelXle (Hübschle et al., 2011) graphical user interface, using the starting parameters obtained in this study under ambient conditions. Neutral scattering factors for Ca, Ir and O were used, and, due to the limited number of unique reflections, all atoms were refined isotropically. Difference Fourier maps show some residual electron density around the Ir atom, given the high electronic number of this atom and the use of an isotropic model. For this reason, uncertainties regarding the oxygen positions are larger than those obtained under ambient conditions but are still sufficiently precise for constraining the high-pressure compression of the $CaIrO_3$ pv structure. A CIF containing all the high-pressure refinements of crystal Ba8x4 is available in the Supplement.

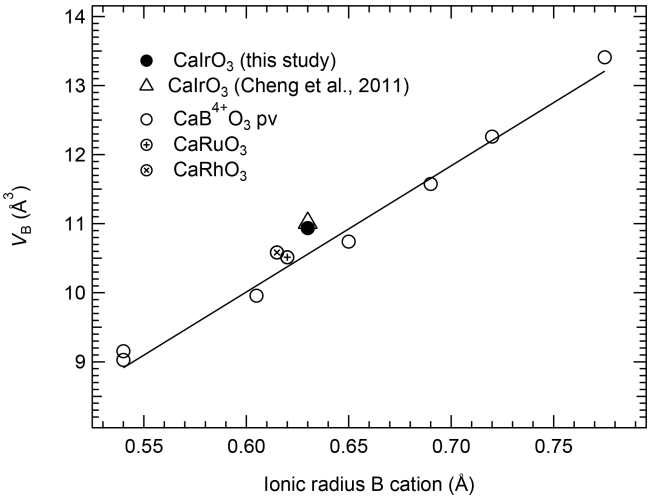

Figure 1. Linear correlation between the octahedral volume, V_B, and the ionic radius of the cation occupying the B site for several $CaB^{4+}O_3$ pv (Table 2) and for $CaIrO_3$ pv investigated in this study and in the study from Cheng et al. (2011). The solid line is a linear weighed fit through the $CaB^{4+}O_3$ perovskite data reported in Table 2. The uncertainties are smaller than the symbol size.

3 Results and discussion

3.1 Structural features of $CaB^{4+}O_3$ perovskites under ambient conditions

The constrained unit-cell lattice parameters of the Ba8x2 sample obtained from a total of 2158 non-unique reflections (Table 1) are within 2σ from those published for another crystal of $CaIrO_3$ pv taken from the same run product (Boffa Ballaran et al., 2007), obtained using the accurate eight-position centring method (Angel et al., 2000; King and Finger, 1979) with a point detector. The structural data obtained in this study are also in good agreement with those obtained from Rietveld refinements of synchrotron powder diffraction data (Cheng et al., 2011).

The octahedral volumes, V_B, of $CaIrO_3$ pv and of several $CaB^{4+}O_3$ perovskites follow, as expected, a linear trend as a function of the ionic radius (Shannon and Prewitt, 1969) of the cation occupying the octahedral site (Fig. 1), increasing from $CaGeO_3$ up to the large $CaPbO_3$ (Table 2). $CaIrO_3$ and, to a lesser extent, $CaRhO_3$ deviate slightly from the trend, though. This deviation is also visible in the variation in the V_B values with the molar volume, V_{mol} (Fig. 2), whereas the volume of the A site, V_A, defined as the volume of the unit cell normalised to the number of formula units minus the volume of the B site ($V_A = V/Z - V_B$), of all the $CaB^{4+}O_3$ perovskites, including $CaIrO_3$, varies linearly as a function of V_{mol} (Fig. 2).

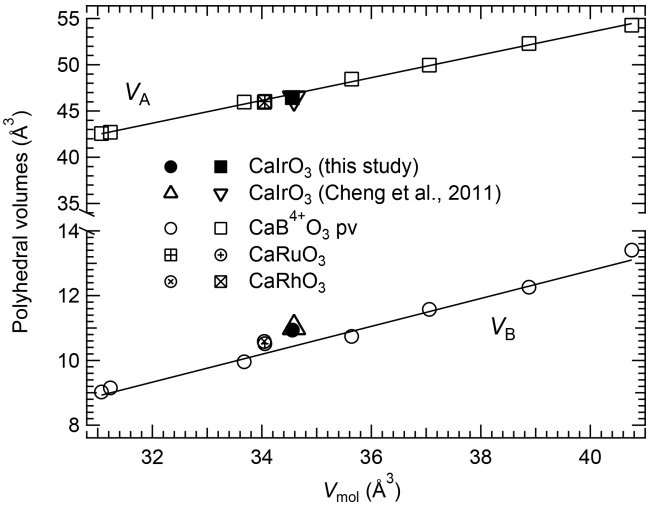

Figure 2. Linear correlation of the octahedral volume, V_B (circles), and the volume of the A site, V_A (squares), with the molar volume, V_{mol}, of several $CaB^{4+}O_3$ pv. The V_B values of $CaIrO_3$ deviate slightly from the linear trend. Solid lines are linear weighed fits through the $CaB^{4+}O_3$ perovskite data reported in Table 2. The uncertainties are smaller than the symbol size.

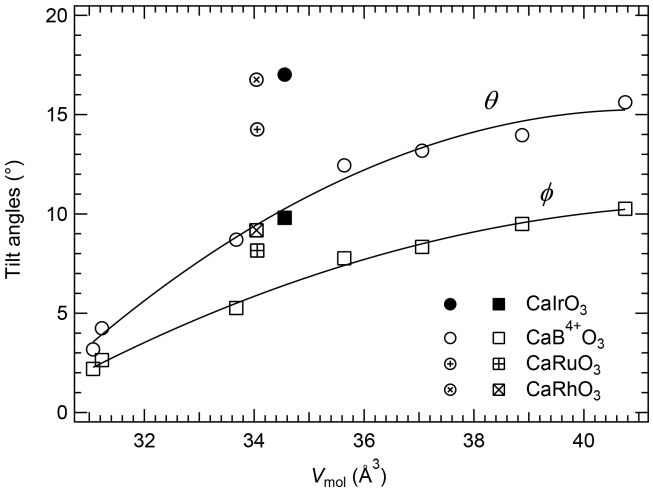

Figure 3. Variation in the out-of-phase, θ (circles), and in-phase, φ (squares), tilts of orthorhombic $CaB^{4+}O_3$ pv as a function of their molar volumes. The tilts of $CaIrO_3$ obtained in this study, as well as those of $CaRuO_3$ and $CaRhO_3$, clearly deviate from the trends. The solid curves are polynomial weighed fits through the $CaB^{4+}O_3$ perovskite data from Table 2, with $CaRhO_3$ and $CaRuO_3$ excluded. The uncertainties are smaller than the symbol size.

The octahedral tilting can be expressed in terms of three tilt angles: θ, φ and Φ (O'Keeffe and Hyde, 1977; Zhao et al., 1993), representing the tilt of the octahedra about the pseudo-cubic $[110]_{pc}$, $[001]_{pc}$ and $[111]_{pc}$ directions of the aristotype $Pm\bar{3}m$ perovskite structure. These can be calculated from the a, b and c unit-cell lattice parameters of the *Pbnm* perovskite structure assuming rigid and non-distorted octahedra according to Zhao et al. (1993):

$$cos\theta = a/b, \tag{1}$$

$$cos\phi = \sqrt{2}a/c, \tag{2}$$

with the Φ tilt being a combination of Eqs. (1) and (2).

$$\cos\Phi = \cos\theta\cos\phi = \frac{\sqrt{2}a^2}{bc} \tag{3}$$

The θ tilt results from the two anti-phase tilts of equal magnitude about the $[100]_{pc}$ and $[010]_{pc}$ directions (Glazer, 1972; Megaw, 1973), and it is indicated as the out-of-phase tilt, whereas the φ tilt results from the tilt about the $[001]_{pc}$ direction and is indicated as the in-phase tilt. The θ and φ tilt angles are plotted as a function of V_{mol} in Fig. 3. The octahedral tilting increases from $CaGeO_3$, for which both tilt angles are close to 3°, to $CaPbO_3$, for which the tilt angles are larger than 10° with $\theta > \varphi$. $CaIrO_3$, $CaRuO_3$ and $CaRhO_3$ have a much more pronounced octahedral tilting, with the out-of-phase tilt having a larger deviation from the trend defined by the other $CaB^{4+}O_3$ perovskites (Fig. 3).

Since the assumption of rigid octahedra is valid only as a first approximation and, moreover, tilting of the octahedral framework also induces a distortion of the A polyhedron, the atomic positions obtained in this study have been used to calculate the Irreps for the *Pbnm* $CaIrO_3$ structure with respect to an ideal cubic perovskite having the same volume using the ISODISTORT programme (Campbell et al., 2006). The same calculations have been performed for the other $CaB^{4+}O_3$ perovskites. As expected, the largest amplitudes computed by the programme are those relative to the symmetry-adapted modes R_4^+ and M_3^+, which are exclusively responsible for the octahedral tilting. From the amplitude of these two symmetry-adapted modes, it is therefore possible to calculate the out-of-phase and in-phase tilts independently of the polyhedral distortion using the equations reported by Wang and Angel (2011):

$$\theta_{R_4^+} = \arctan\left(2d'_{R_4^+}\right), \tag{4}$$

$$\phi_{M_3^+} = \arctan\left(2d'_{M_3^+}\right), \tag{5}$$

where d' is derived from the output of ISODISTORT following the procedure outlined by Wang and Angel (2011) (see their example for $MgSiO_3$ bridgmanite).

The variations with V_{mol} of $\theta_{R_4^+}$ and $\phi_{M_3^+}$ (Fig. 4) are different from the tilting patterns obtained using the unit-cell lattice parameter values (Fig. 3). Not only is their variation with the molar volume of the $CaB^{4+}O_3$ perovskites linear, but the values of the in-phase and out-of-phase tilts are also very similar for all analysed samples. However, similarly to what was observed for the tilts obtained from the unit-cell parameters, the values calculated for $CaIrO_3$, $CaRhO_3$ and $CaRuO_3$ are much larger and deviate from the trend described by the other $CaB^{4+}O_3$ perovskites. The difference between the two sets of calculations is due to the fact that the

Table 1. Unit-cell lattice parameters and polyhedral volumes of the $CaIrO_3$ perovskite-type phase measured under ambient conditions and high pressure (*Pbnm* space group).

	a (Å)	b (Å)	c (Å)	V (Å^3)	V_B (Å^3)	V_A (Å^3)
$CaIrO_3$ (ref. 1)	5.34765 (10)	5.59186 (9)	7.6735 (2)	229.463 (8)	–	–
$CaIrO_3$ (ref. 2)	5.35046 (1)	5.59291 (1)	7.67694 (2)	229.730 (1)	11.011 (9)	46.421 (9)
Ba8x2	5.3485 (2)	5.5928 (2)	7.6731 (2)	229.53 (2)	10.936 (15)	46.446 (16)
Pressure measurements of $CaIrO_3$ (Ba8x4)						
P (GPa)	a (Å)	b (Å)	c (Å)	V (Å^3)	V_B (Å^3)	V_A (Å^3)
0.0001	5.3456 (9)	5.5854 (16)	7.680 (4)	229.30 (14)	10.95 (5)	46.38 (7)
2.16 (10)	5.3171 (12)	5.5748 (19)	7.647 (4)	226.66 (16)	10.88 (5)	45.78 (7)
3.70 (10)	5.2936 (10)	5.5636 (17)	7.618 (3)	224.35 (15)	10.68 (6)	45.41 (7)
6.41 (10)	5.2593 (13)	5.552 (2)	7.588 (4)	221.60 (16)	10.62 (6)	44.78 (7)
7.20 (10)	5.2495 (12)	5.5511 (18)	7.579 (4)	220.86 (15)	10.50 (5)	44.72 (6)
9.70 (10)	5.2183 (11)	5.5425 (17)	7.540 (4)	218.06 (13)	10.46 (7)	44.07 (9)

Ref 1: Boffa Ballaran et al. (2007). Ref. 2: Cheng et al. (2011).

Table 2. Unit-cell lattice parameters and polyhedral volumes of $CaB^{4+}O_3$ perovskite-type phases reported in the literature (*Pbnm* space group).

	a (Å)	b (Å)	c (Å)	V (Å^3)	V_B (Å^3)	V_A (Å^3)	References
$CaGeO_3$	5.2607 (6)	5.2688 (10)	7.4452 (15)	206.36 (6)	9.026 (5)	42.564 (9)	Sasaki et al. (1983)
$CaMnO_3$	5.2671 (1)	5.2816 (1)	7.4567 (1)	207.44 (1)	9.154 (5)	42.706 (8)	Božin et al. (2008)
$CaTiO_3$	5.3796 (1)	5.4423 (3)	7.6401 (5)	223.68 (1)	9.956 (3)	45.964 (6)	Sasaki et al. (1987)
$CaRhO_3$	5.3267 (1)	5.5631 (1)	7.6308 (1)	226.12 (1)	10.58 (2)	45.95 (3)	Shirako et al. (2009)
$CaRuO_3$	5.354 (1)	5.524 (1)	7.649 (1)	226.2 (1)	10.52 (1)	46.04 (2)	Bensch et al. (1990)
$CaMoO_3$	5.4510 (1)	5.5821 (1)	7.7803 (2)	236.73 (9)	10.741 (6)	48.442 (9)	De La Calle et al. (2006)
$CaSnO_3$	5.5142 (2)	5.6634 (2)	7.8816 (2)	246.14 (2)	11.576 (5)	49.96 (1)	Zhao et al. (2004a)
$CaZrO_3$	5.59111 (7)	5.76128 (8)	8.0169 (1)	258.24 (1)	12.261 (3)	52.299 (4)	Levin et al. (2003)
$CaPbO_3$	5.661 (1)	5.878 (1)	8.136 (1)	270.7 (1)	13.409 (7)	54.266 (8)	Yamamoto et al. (1999)

polyhedral distortion in these perovskites is not negligible; nevertheless, even as just a first approximation, the tilt angles obtained from the unit-cell lattice parameters, based on the assumption of rigid and undistorted polyhedra, already highlight the distinctive behaviour of perovskites having a Pt-group element (i.e. Ir, Ru and Rh) occupying the octahedral site.

The polyhedral distortion is mainly due to the symmetry-adapted mode X_5^+ and, in particular, the displacement of the Ca atoms (X_5^+ A) (Fig. 5), since the amplitudes of the symmetry-adapted modes R_5^+ and M_2^+ are practically negligible. The distortion of the A-site polyhedron increases due to the displacement of the Ca atoms toward one side of the cavity, probably in order to have better coordination with at least some of the oxygen atoms, as a consequence of the octahedral frameworks becoming larger with the increasing size of the cation occupying the B site. However, the A sites of $CaIrO_3$, $CaRuO_3$ and $CaRhO_3$ perovskites appear much more distorted than expected from the size of the octahedral cations. The above observations, therefore, suggest that, in the case of the CaO orthorhombic perovskite structures, octahedral tilting and distortion result primarily from the mismatch of the B- and A-cation sizes, whereas, in the case of the Pt-group element perovskites, the B site appears larger than expected, giving rise to a larger orthorhombic distortion. This behaviour may be due to the small difference in electronegativity between the Pt-group elements and the oxygen, causing a weaker and therefore longer-than-expected ionic bond at the octahedral site.

$CaIrO_3$, $CaRuO_3$ and $CaRhO_3$ perovskites transform under high pressure to a post-perovskite phase (orthorhombic *Cmcm* $CaIrO_3$-type structure), which is either the stable phase under ambient pressure ($CaIrO_3$) or the metastable phase that is easily quenchable (Hirose and Fujita, 2005; Kojitani et al., 2007a, b; Shirako et al., 2009). A *Cmcm* $CaIrO_3$-type structure has also been found for $CaPtO_3$ (Inaguma et al., 2008); however, no report of a perovskite structure of this compound is present in the literature.

Akaogi et al. (2010) have reported that there is an inverse correlation between the transition pressure of these perovskites and the tilt angle Φ (Eq. 3). $CaSnO_3$ pv has a Φ angle similar to that of $CaRuO_3$ pv, and it has been re-

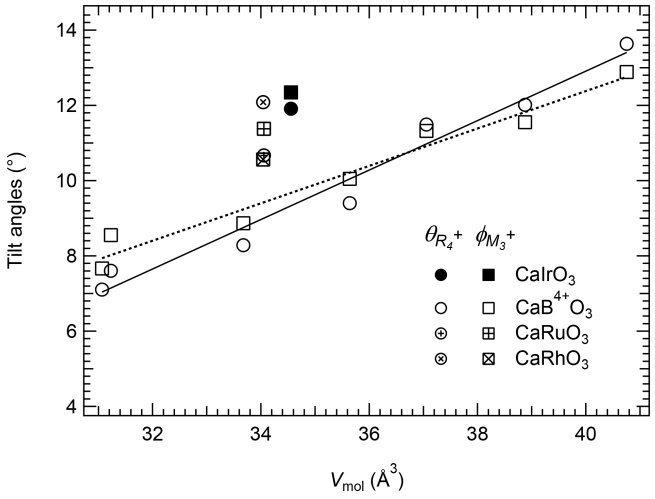

Figure 4. Variation in the out-of-phase, $\theta_{R_4^+}$, and in-phase, $\varnothing_{M_3^+}$, tilts calculated from the symmetry-adapted R_4^+ and M_3^+ mode amplitudes for $CaB^{4+}O_3$ pv. Note that the values obtained for $CaIrO_3$, $CaRuO_3$ and $CaRhO_3$ clearly deviate from the trends described by the other $CaB^{4+}O_3$ pv. The estimated uncertainties are smaller than the symbol size. The solid and dotted lines are linear weighed fits through the $\theta_{R_4^+}$ and $\varnothing_{M_3^+}$ $CaB^{4+}O_3$ perovskite data, respectively.

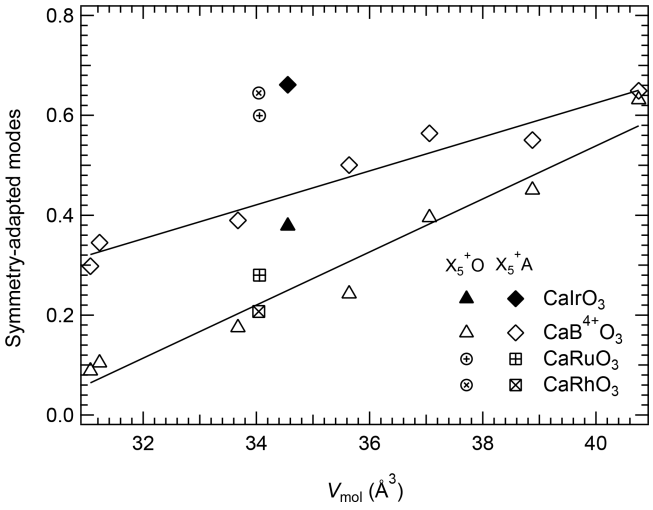

Figure 5. Variation with molar volume in the amplitude of the symmetry-adapted modes X_5^+ relative to the displacement of the oxygen, X_5^+O, and Ca atoms, X_5^+A, from the ideal positions of the aristotype cubic structure for $CaB^{4+}O_3$ pv. The values obtained for $CaIrO_3$, $CaRhO_3$ and $CaRuO_3$ deviate from the trends described by the other $CaB^{4+}O_3$ pv. Solid lines are linear weighed fits through the $CaB^{4+}O_3$ pv data.

ported to transform to a post-perovskite structure (Tateno et al., 2010) that can be quenched under room conditions, albeit just as a mixture of perovskite and post-perovskite phases rather than a single phase as for the other three perovskites. The transition, however, occurs above 40 GPa, i.e. at pressures much larger than expected from the Φ tilt trend defined by the Pt-group perovskites (Akaogi et al., 2010), suggesting that not only octahedral tilting but also polyhedral distortion may play a significant role in determining the pressure at which the perovskite-to-post-perovskite phase transformation occurs. The large tilting and polyhedral distortion may also significantly affect the compressibility of these three perovskites, making them stiffer than expected, as observed for $CaIrO_3$ pv (Boffa Ballaran et al., 2007).

3.2 Compression mechanism of $CaB^{4+}O_3$ perovskites

The unit-cell lattice parameters of the Ba8x4 crystal loaded in the DAC under room pressure before loading the pressure-transmitting medium were obtained from a total of 354 non-unique reflections and are in good agreement with those determined for the Ba8x2 crystal (Table 1). The bulk compression behaviour of the Ba8x4 crystal is also in agreement with the equation of state determined by Boffa Ballaran et al. (2007), confirming that $CaIrO_3$ pv is much stiffer than other $CaB^{4+}O_3$ perovskites (Boffa Ballaran et al., 2007; Ross and Chaplin, 2003). The high-pressure structural evolution of non-cubic ABO_3 perovskites under hydrostatic conditions depends on the relative compression of the BO_6 octahedra and AO_{12} polyhedra (e.g. Zhao et al., 2004b), with consequent change in octahedral tilting. For $A^{2+}B^{4+}O_3$ perovskites, the BO_6 octahedra are expected to be less compressible than the AO_{12} polyhedra, and the octahedral tilting is therefore expected to increase with pressure. This is the case for $CaSnO_3$ (Zhao et al., 2004a) and $CaTiO_3$ (Zhao et al., 2011), for which it was shown that the V_A/V_B ratio decreases with increasing pressure. In contrast, the V_A/V_B ratio obtained in this study for $CaIrO_3$ pv appears to be independent of pressure (Fig. 6). A weighed linear fit through the data even suggests a slight increase in the V_A/V_B ratio with pressure, implying that the octahedral site of $CaIrO_3$ pv has a compressibility similar to or even larger than that of the A site, in contrast to the observed trend for the other two $CaB^{4+}O_3$ perovskites.

Since the V_A/V_B ratio can be used to describe the octahedral tilting of orthorhombic perovskites, i.e. the larger the tilt, the larger the deviation of the V_A/V_B ratio from the ideal value of 5 in the cubic aristotype perovskite, it appears that the orthorhombic distortion of $CaIrO_3$ due to octahedral tilting remains constant at least up to 10 GPa, in contrast to the other two $CaB^{4+}O_3$ perovskites, whose tilting increases with pressure (Zhao et al., 2004a, 2011).

This behaviour is quite surprising since it has been suggested that the perovskite-to-post-perovskite transformation is driven by the repulsion between inter-octahedral anions, which become closer due to the increasing octahedral tilting with pressure. Martin and Parise (2008) analysed the structural data of 70 perovskites under ambient and high-

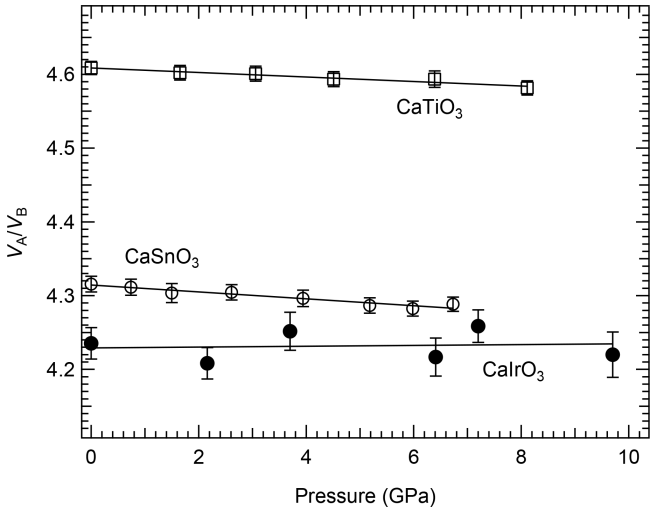

Figure 6. Variation with pressure in the V_A/V_B ratio of $CaIrO_3$ pv (this study) compared with values for $CaSnO_3$ (Zhao et al., 2004a) and $CaTiO_3$ (Zhao et al., 2011). In contrast to what is expected for $A^{2+}B^{4+}O_3$ perovskites, the V_A/V_B ratio of $CaIrO_3$ pv is independent of pressure, at least in the pressure range investigated in this study.

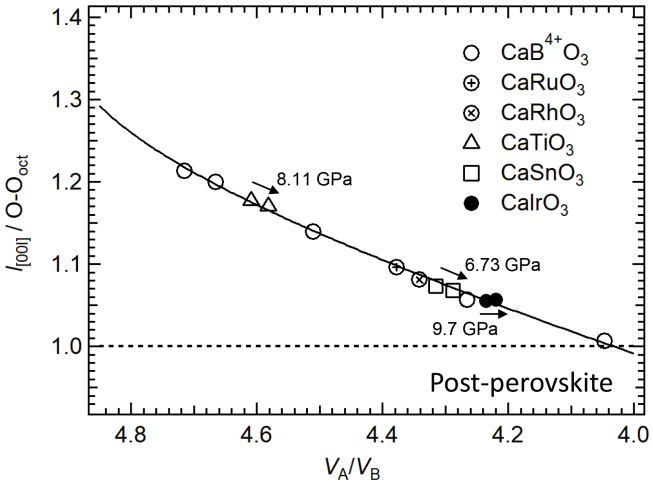

Figure 7. Variation with the V_A/V_B ratio in the inter-oxygen distances $l_{[001]}$ along the c axis, normalised with respect to the intra-oxygen distance of the accompanying octahedral site, O–O_{oct}, for the $CaB^{4+}O_3$ pv. The high-pressure values for $CaIrO_3$ pv (this study), $CaSnO_3$ (Zhao et al., 2004a) and $CaTiO_3$ (Zhao et al., 2011) are also reported. The solid line is the mathematical model reported by Martin and Parise (2008).

temperature or high-pressure conditions and suggested that a minimum V_A/V_B ratio of ~ 4.03 should be reached in order for the inter-octahedral anion distances to be equal to the intra-octahedral anion distances, hence causing the transition to post-perovskite. These authors show that the V_A/V_B ratio decreases and octahedral tilting increases with pressure not only for $CaSnO_3$, but also for other perovskite-structured materials, for example $NaMgF_3$ and $SrCeO_3$. This is also valid for the end-member $MgSiO_3$ bridgmanite and Al-bearing bridgmanite, for which it has been found that the A site is more compressible than the B site (Criniti et al., 2024). Following Martin and Parise (2008), the distances $l_{[001]}$ between the oxygens in the 8d Wyckoff position along the c axis of the $CaB^{4+}O^3$ perovskites, normalised with respect to the intra-oxygen distance of the accompanying octahedral site, O–O_{oct}, are reported as a function of the V_A/V_B ratio for the $CaB^{4+}O_3$ perovskites (Fig. 7). The $l_{[001]}$/ O–O_{oct} distances of $CaTiO_3$ at 8.11 GPa of $CaSnO_3$ at 6.73 GPa and $CaIrO_3$ at 9.7 GPa are also reported in the same figure. All data points closely follow the mathematical model defined by Martin and Parise (2008), likely due to the fact that this inter-anion distance is not sensitive to deformation of the octahedra, as already noted by those authors.

There are, however, two important points to be made: (i) the $l_{[001]}$/ O–O_{oct} values of $CaRuO_3$ and $CaRhO_3$ are larger than those of $CaSnO_3$; therefore if tilting alone was driving the perovskite-to-post-perovskite transition, one would expect a higher transition pressure for $CaRuO_3$ and $CaRhO_3$ than for $CaSnO_3$, contrary to what has been reported, and (ii) in spite of the smaller pressure range investigated for $CaTiO_3$ and $CaSnO_3$, the change in $l_{[001]}$/ O–O_{oct} due to increasing pressure is much more accentuated for these two perovskites than for $CaIrO_3$ (this study), confirming that the octahedral tilting for $CaIrO_3$ does not change at least up to 10 GPa. This suggests that for $CaIrO_3$, and likely also for the other Pt-group perovskite-structured materials, octahedral tilts alone are not sufficient to explain the mechanism for the perovskite-to-post-perovskite transition. A major factor driving the phase transformation appears to be the displacement of the Ca atoms, which is already quite large under room conditions for the Pt-group element perovskites (Fig. 5) and increases significantly with pressure for $CaIrO_3$ relative to the displacement of Ca in the $CaSnO_3$ structure (Fig. 8).

It is very likely that, as the Ca atoms are displaced toward one side of the large A site in $CaIrO_3$ pv, some of the Ca–O bond distances become shorter, giving rise to a much stiffer A site with respect to that of the $CaSnO_3$ structure. Because the octahedral tilting in $CaIrO_3$ is hindered by such polyhedral distortion, we can expect that the structure becomes more unstable under compression, favouring the transformation to the post-perovskite phase at pressures lower than would be expected if octahedral tilting alone were the main cause of the transition.

4 Conclusions

Refinements to single-crystal intensity data collected under both ambient and high-pressure conditions have allowed us to clarify the tilting and distortion of orthorhombic $CaIrO_3$ pv. Both octahedral tilting (Figs. 3 and 4) and A-

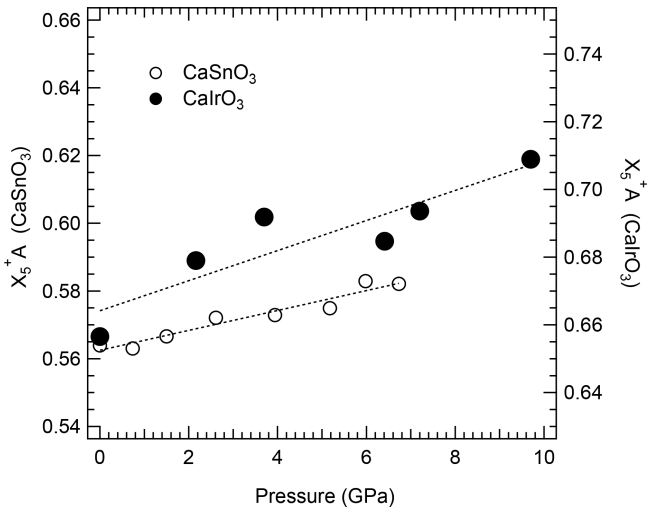

Figure 8. Variation with pressure in the amplitude of the symmetry-adapted modes X_5^+ relative to the displacement of the Ca atoms, X_5^+A, from the positions of the aristotype cubic structure for $CaSnO_3$ (left axis) and $CaIrO_3$ pv (right axis). The scale of the two axes is identical to better visualise the larger increase in the distortion of $CaIrO_3$ compared to $CaSnO_3$. The dotted lines are guides to eye. Uncertainties are smaller than the symbol sizes.

site distortion (Fig. 5) of this perovskite are much larger with respect to other $CaB^{4+}O_3$ perovskites, causing the $CaIrO_3$ structure to be much stiffer than expected. The larger tilting and distortion appear to be characteristic of orthorhombic perovskites with a Pt-group element (i.e. Ir, Ru and Rh) occupying the octahedral site. Although there are no compressibility data for $CaRuO_3$ and $CaRhO_3$, it can be expected that the bulk modulus will also be larger than the trend shown by several other $CaB^{4+}O_3$ perovskites (Ross and Chaplin, 2003) for these two perovskites. Another peculiarity of the $CaIrO_3$ structure is represented by the fact that the B and A sites have similar compressibility, at least up to 10 GPa, resulting in the octahedral tilt remaining constant instead of increasing with increasing pressure. The similar compression of the two sites may hinder oxygen–oxygen repulsion, which is the main factor responsible for stiffening the perovskite structure with increasing pressure, giving rise to a bulk modulus first pressure derivative, K', smaller than 4. Ultimately, we can hypothesise that the relatively large stiffness of $CaIrO_3$, the similar compressibility of the B and A sites, and the large distortion of the A-site polyhedron play an important role in determining the transformation pressure at which the perovskite structure transforms to the orthorhombic *Cmcm* post-perovskite and therefore should be a common feature of the Pt-group perovskites for which the same transformation has been reported (Akaogi et al., 2010).

Code and data availability. All of the crystallographic data have been made available in the Supplement.

Supplement. The supplement related to this article is available online at https://doi.org/10.5194/ejm-37-699-2025-supplement.

Author contributions. TBB helped with the selection of the single crystals of $CaIrO_3$ pv, analysed the data and wrote the first draft of the paper. KK prepared the diamond anvil for the high-pressure study, collected all single-crystal diffraction data and contributed to the final version of the paper. RGT synthesised and characterised the high-quality single crystals of $CaIrO_3$ pv and contributed to the final version of the paper.

Competing interests. At least one of the (co-)authors is a member of the editorial board of *European Journal of Mineralogy*. The peer-review process was guided by an independent editor, and the authors also have no other competing interests to declare.

Disclaimer. Publisher's note: Copernicus Publications remains neutral with regard to jurisdictional claims made in the text, published maps, institutional affiliations, or any other geographical representation in this paper. While Copernicus Publications makes every effort to include appropriate place names, the final responsibility lies with the authors.

Special issue statement. This article is part of the special issue "Celebrating the outstanding contribution of Paola Bonazzi to mineralogy". It is not associated with a conference.

Acknowledgements. The authors thank Alexander Kurnosov for help with the diamond anvil cell loading. We also thank an anonymous reviewer, M. Akaogi and Wilson Crichton in particular for their useful suggestions.

Financial support. The Centre for Planetary Habitability is funded by CoE grant no. 332523 from the Research Council of Norway. This research has been supported by the Deutsche Forschungsgemeinschaft (grant no. BO2550/4-2).

Review statement. This paper was edited by Luca Bindi and reviewed by M. Akaogi, Wilson Crichton, and one anonymous referee.

References

Akaogi, M., Shirako, Y., Kojitani, H., Takamori, S., Yamaura, K., and Takayama-Muromachi, E.: Post-perovskite transitions in

$CaB^{4+}O_3$ at high pressure, J. Phys. Conf. Ser., 215, 012095, https://doi.org/10.1088/1742-6596/215/1/012095, 2010.

Angel, R. J., Downs, R. T., and Finger, L. W.: High-temperature-high-pressure diffractometry, in: High-Temperature and High-Pressure Crystal Chemistry, edited by: Hazen, R. M. and Downs, R. T., 41, 559–596, Reviews in Mineralogy, Mineralogical Society of America, Chantilly, Virginia, ISBN 0-939950-53-7, 2000.

Angel, R. J.: Absorption corrections for diamond-anvil pressure cells implemented in the software package Absorb6.0, J. Appl. Cryst., 37, 486–492, https://doi.org/10.1107/S0021889804005229, 2004.

Bensch, W., Schmalle, H. W., and Reller, A.: Structure and thermochemical reactivity of $CaRuO_3$ and $SrRuO_3$, Solid State Ionics, 43, 171–177, https://https://doi.org/10.1016/0167-2738(90)90481-6, 1990.

Boffa Ballaran, T., Trønnes, R. G., and Frost, D. J.: Equations of state of $CaIrO_3$ perovskite and post-perovskite phases, Am. Mineral., 92, 1760–1763, https://doi.org/10.2138/am.2007.2715, 2007.

Božin, E. S., Sartbaeva, A., Zheng, H., Wells, S. A., Mitchell, J. F., Proffen, Th., Thorpe, M.F., and Billinge, S. J. L.: Structure of $CaMnO_3$ in the range $10\,K \leq T \leq 550\,K$ from neutron time-of-flight total scattering, J. Phys. Chem. Solid., 69, 2146–2150, https://doi.org/10.1016/j.jpcs.2008.03.029, 2008.

Campbell, B. J., Stokes, H. T., Tanner, D. E., and Hatch, D. M.: ISODISPLACE: A web-based tool for exploring structural distortions, J. Appl. Cryst., 39, 607–614, https://doi.org/10.1107/S0021889806014075, 2006.

Cheng, J.-G., Zhou, J.-S., Goodenough, J. B., Sui, Y., Ren, Y., and Suchomel, M. R.: High-pressure synthesis and physical properties of perovskite and post-perovskite $Ca_{1-x}Sr_xIrO_3$, Phys. Rev. B, 83, 064401, https://doi.org/10.1103/PhysRevB.83.064401, 2011.

Clark, R. C. and Reid, J. S.: The Analytical Calculation of Absorption in Multifaceted Crystals, Acta Cryst. A, 51, 887–897, https://doi.org/10.1107/S0108767395007367, 1995.

Criniti, G., Boffa Ballaran, T., Kurnosov, A., Liu, Z., Glazyrin, K., Merlini, M., Hanfland, M., and Frost, D. J.: Thermal Equation of State and Structural Evolution of Al-bearing Bridgmanite. J. Geophys. Res.-Sol. Ea., 129, e2023JB026879, https://https://doi.org/10.1029/2023JB026879, 2024

de la Calle, C., Alonso, J. A., García-Hernández, M., and Pomjakushin, V.: Neutron diffraction study and magnetotransport properties of stoichiometric $CaMoO_3$ perovskite prepared by a soft-chemistry route, J. Solid State Chem., 179, 1636–1641, https://doi.org/10.1016/j.jssc.2006.02.022, 2006.

Finger, L. W. and King, H. E.: A revised method of operation of the single-crystal diamond cell and refinement of structure of NaCl at 32 kbar, Am. Mineral., 63, 337–342, 1978.

Glazer, A.: The classification of tilted octahedra in perovskites, Acta Cryst. B, 28, 3384–3392, https://doi.org/10.1107/S0567740872007976, 1972.

Hirose, K. and Fujita, Y.: Clapeyron slope of the post-perovskite phase transition in $CaIrO_3$, Geophys. Res. Lett., 32, L13313, https://doi.org/10.1029/2005GL023219, 2005.

Howard, C. J. and Stokes, H. T.: Group-theoretical analysis of octahedral tilting in perovskites, Acta Cryst. B, 54, 782–789, https://doi.org/10.1107/S0108768198004200, 1998.

Howard, C. J. and Stokes, H. T.: Group-Theoretical Analysis of Octahedral Tilting in Perovskites, Erratum, Acta Cryst. B, 58, 565–565, https://https://doi.org/10.1107/S010876810200890X, 2002.

Huang, R., Boffa Ballaran, T., McCammon, C. A., Miyajima, N., and Frost, D. J.: The effect of Fe-Al substitution on the crystal structure of $MgSiO_3$ bridgmanite, J. Geophys. Res.-Sol. Ea., 126, e2021JB021936, https://doi.org/10.1029/2021JB021936, 2021.

Hübschle, C. B., Sheldrick, G. M., and Dittrich, B.: ShelXle: a Qt graphical user interface for SHELXL, computer programs, J. Appl. Cryst., 44, 1281-1284, https://doi.org/10.1107/S0021889811043202, 2011.

Inaguma, Y., Hasumi, K.-I., Yoshida, M., Ohba, T., and Katsumata, T.: High-Pressure Synthesis, Structure, and Characterization of a Post-perovskite $CaPtO_3$ with $CaIrO_3$-Type Structure, Inorg. Chem., 47, 1868–1870, https://doi.org/10.1021/ic701851e, 2008.

Kantor, I., Prakapenka, V., Kantor, A., Dera, P., Kurnosov, A., Sinogeikin, S., Dubrovinskaia, N., and Dubrovinsky, L.: BX90: A new diamond anvil cell design for X-ray diffraction and optical measurements, Rev. Sci. Instrum., 83, 125102, https://doi.org/10.1063/1.4768541, 2012.

King, H. and Finger, L.: Diffracted beam crystal centering and its application to high-pressure crystallography, J. Appl. Cryst., 12, 374–378, https://doi.org/10.1107/S0021889879012723, 1979.

Kojitani, H., Furukawa, A., and Akaogi, M.: Thermochemistry and high-pressure equilibria of the post-perovskite phase transition in $CaIrO_3$, Am. Mineral., 92, 229–232, https://doi.org/10.2138/am.2007.2358, 2007a.

Kojitani, H., Shirako, Y., and Akaogi, M.: Post-perovskite phase transition in $CaRuO_3$, Phys. Earth Plan. Int., 165, 127–134, https://doi.org/10.1016/j.pepi.2007.09.003, 2007b.

Kurnosov, A., Kantor, I., Boffa Ballaran, T., Lindhardt, S., Dubrovinsky, L., Kuznetsov, A., and Zehnder, B. H.: A novel gas-loading system for mechanically closing of various types of diamond anvil cells, Rev. Sci. Instrum., 79, 045110, https://doi.org/10.1063/1.2902506, 2008.

Levin, I., Amos, T. G., Bell, S. M., Farber, L., Vanderah, T. A., Roth, R. S., and Toby, B. H.: Phase equilibria, crystal structures, and dielectric anomaly in the $BaZrO_3$-$CaZrO_3$ system, J. Solid State Chem., 175, 170–181, https://doi.org/10.1016/S0022-4596(03)00220-2, 2003.

Marbouh, N., Belabbes, M., Khelfaoui, F., Khalfallah, B., Bentayeb, A., and Driss Khodja, M.: Computational study of the structural, elastic, electronic and thermoelectric properties of the orthorhombic perovskite $CaIrO_3$ compound, Comput. Condens. Matter, 29, e00594, https://https://doi.org/10.1016/j.cocom.2021.e00594, 2021.

Martin, C. D. and Parise, J. B.: Structure constraints and instability leading to the post-perovskite phase transition of $MgSiO_3$, Earth Planet. Sc. Lett., 265, 630–640, https://doi.org/10.1016/j.epsl.2007.11.001, 2008.

McDaniel, C. L. and Schneidler, S. J.: Phase relations in the CaO-IrO_2-Ir system in air, J. Solid State Chem., 4, 275–280, https://doi.org/10.6028/jres.075A.019, 1972.

Megaw, H. D.: Crystal Structures-A Working Approach, Saunders, Philadelphia, ISBN-10 0721662609, 1973.

Miller, S. C. and Love, W. F.: Tables of Irreducible Representations of Space Groups and Co-representations of Magnetic Space Groups, Boulder, Colarado, Pruett, 1967.

Mitchell, R. H.: Perovskites: Modern and ancient, Almaz Press, ISBN 0-9689411-0-9, 2002.

Murakami, M., Hirose, K., Kawamura, K., Sata, N., and Ohishi, Y.: Postperovskite phase transition in $MgSiO_3$, Science, 304, 855–858, https://doi.org/10.1126/science.1095932, 2004.

Oganov, A. R. and Ono, S.: Theoretical and experimental evidence for a postperovskite phase of $MgSiO_3$ in Earth's D″ layer, Nature, 430, 445–448, https://doi.org/10.1038/nature02701, 2004.

O'Keeffe, M. and Hyde, B. G.: Some structures topologically related to cubic perovskite ($E2_1$), ReO_3 ($D0_9$) and Cu_3Au ($L1_2$), Acta Cryst. B, 33, 3802–3813, https://doi.org/10.1107/S0567740877012114, 1977.

O'Keeffe, M., Hyde, B. G., and Bovin, J.O.: Contribution to the crystal chemistry of orthorhombic perovskite: $MgSiO_3$ and $NaMgF_3$, Phys. Chem. Minerals, 4, 299–305, 1979.

Perez-Mato, J. M., Orobengoa, D., and Aroyo, M. I.: Mode crystallography of distorted structures, Acta Cryst. A, 66, 558–590, https://doi.org/10.1107/S0108767310016247, 2010.

Ross, N. L. and Chaplin, T. D.: Compressibility of $CaZrO_3$ perovskite: Comparison with Ca-oxide perovskites, J. Solid State Chem., 172, 123–126, https://doi.org/10.1016/S0022-4596(02)00166-4, 2003.

Sasaki, S., Prewitt, C. T., and Liebermann, R. C.: The crystal structure of $CaGeO_3$ perovskite and the crystal chemistry of the $GdFeO_3$-type perovskites, Am. Mineral., 68, 1189–1198, 1983.

Sasaki, S., Prewitt, C. T., Bass, J. D., and Schulze, W. A.: Orthorhombic Perovskite $CaTiO_3$ and $CdTiO_3$: Structure and Space Group, Acta Cryst. C, 43, 1668–1674, 1987.

Shannon, R. D. and Prewitt, C. T.: Effective Ionic Radii in Oxides and Fluorides, Acta Cryst. B, 25, 925–946, https://doi.org/10.1107/S0567740869003220, 1969.

Sheldrick, G. M.: Crystal structure refinement with SHELXL, Acta Cryst. C, 71, 3–8, https://doi.org/10.1107/S2053229614024218, 2015.

Shen, G., Wang, Y., Dewaele, A., Wu, C., Fratanduono, D. E., Eggert, J., Klotz, S., Dziubek, K. F., Loubeyre, P., Fat'yanov, O. V., Asimow, P. D., Mashimo, T., Wentzcovitch, R. M. M., and other members of the IPPS task group: Toward an international practical pressure scale: A proposal for an IPPS ruby gauge (IPPS-Ruby2020), High Press. Res., 40, 299–314, https://doi.org/10.1080/08957959.2020.1791107, 2020.

Shirako, Y., Kojitani, H., Akaogi, M., Yamaura, K., and Takayama-Muromachi, E.: High-pressure phase transitions of $CaRhO_3$ perovskite, Phys. Chem. Minerals, 36, 455–462, https://doi.org/10.1007/s00269-009-0292-4, 2009.

Stølen, S. and Trønnes R. G.: The perovskite to post-perovskite transition in $CaIrO_3$: Clapeyron slope and changes in bulk and shear moduli by density functional theory, Phys. Earth Planet. Int., 164, 50–62, https://doi.org/10.1016/j.pepi.2007.05.009, 2007.

Tateno, S., Hirose, K., Sata, N., and Ohishi, Y.: Structural distortion of $CaSnO_3$ perovskite under pressure and the quenchable post-perovskite phase as a low-pressure analogue to $MgSiO_3$, Phys. Earth Planet. Int., 181, 54–59, https://https://doi.org/10.1016/j.pepi.2010.03.003, 2010.

Trønnes, R. G., Frost, D. J., Boffa Ballaran, T., and Stølen, S.: The perovskite to post-perovskite transition in $CaIrO_3$, American Geophysical Union Fall Meeting, MR11A97, 2006.

Wang, D. and Angel, R. J.: Octahedral tilts, symmetry-adapted displacive modes and polyhedral volume ratios in perovskite structures, Acta Cryst. B, 67, 302–314, https://doi.org/10.1107/S0108768111018313, 2011.

Yamamoto, A., Khasanova, N. R., Izumi, F., Wu, X.-J., Kamiyama, T., Torii, S., and Tajima, S.: Crystal Structure and Its Role in Electrical Properties of the Perovskite $CaPbO_3$ Synthesized at High Pressure, Chem. Mater., 11, 747–753, https://doi.org/10.1021/cm980629p, 1999.

Zhao, J., Ross, N. L., and Angel, R.J.: Tilting and distortion of $CaSnO_3$ perovskite to 7 GPa determined from single-crystal X-ray diffraction, Phys. Chem. Minerals, 31, 299–305, https://doi.org/10.1007/s00269-004-0391-1, 2004a.

Zhao, J., Ross, N. L., and Angel, R. J.: New view of the high-pressure behaviour of $GdFeO_3$-type perovskites, Acta Cryst. B, 60, 263–271, https://doi.org/10.1107/S0108768104004276, 2004b.

Zhao, J., Ross, N. L., Wang, D., and Angel, R. J.: High-pressure crystal structure of elastically isotropic $CaTiO_3$ perovskite under hydrostatic and non-hydrostatic conditions, J. Phys.: Condens. Matter, 23, 455401, https://doi.org/10.1088/0953-8984/23/45/455401, 2011.

Zhao, Y., Weidner, D. J., Parise, J. B., and Cox, D. E.: Thermal expansion and structural distortion of perovskite-Data for $NaMgF_3$ perovskite, Part I, Phys. Earth Planet. Int., 76, 1–34, https://doi.org/10.1016/0031-9201(93)90051-A, 1993.